The University of Santa Clara • California

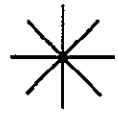

INVESTIGATION OF THE USE OF THE KERR MAGNETO-OPTIC EFFECT FOR THE MEASUREMENT OF MAGNETIC FIELDS

By

Dr. Raymond B. Yarbrough and Frank S. Greene, Jr.

April 1969

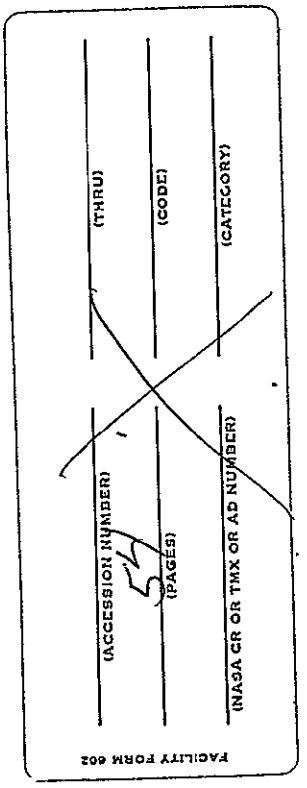

FINAL REPORT - PHASE II

Prepared under Contract No. b6/T1-C/S.C. Omni. #010 for

AMES RESEARCH CENTER
NATIONAL AERONAUTICS AND SPACE ADMINISTRATION

by

The University of Santa Clara
Santa Clara, California

TABLE OF CONTENTS

NOMENCLATURE

$\mathring{A}$	-	angstrom (10^{-10} meters)
A_1	-	fraction of illuminated film area with positive magnetization
A_2	-	fraction of illuminated film area with negative magnetization
A_T	-	total illuminated film area
ΔA	-	difference between A_1 and A_2
a	-	aperture of lense
B	-	cone angle of scattered light
C.C.	-	common collector
C.E.	-	common emitter
d	-	diameter
d.b.	-	decibel
E_{pi}	-	magnitude of the incident electric vector of p-light
E_{pr}	-	magnitude of the reflectal electric vector of p-light
E_{si}	-	magnitude of the incident electric vector of s-light
E_{sr}	-	magnitude of the reflected electric vector of s-light
e.a.	-	easy axis
e_{nb}	-	base thermal noise voltage
e_{nc}	-	collector shot noise voltage referred to the base
Fe	-	iron
f	-	frequency
f	-	focal length (section 3.3)
Δf	-	bandwidth
g_m	-	transconductance
H_k	-	Anistropy field
H_{ki}	-	local value of anisotropy field

NOMENCLATURE (Con't.)

H_L - longitudinal or easy-axis component of magnetic field

H_{sat} - longitudinal magnetic field necessary to cause saturation

H_T - transvere or hard-axis component of magnetic field

HZ - Hertz, cycles per second

I - current in photo-device

I_b - d.c. value of base current

I_c - d.c. value of emitter current

I_D - intensity of light incident on photodetector

I_d - diode current

I_o - intensity of light reflected from film

I.D. - inside diameter

i_c - collector signal plus noise current

i_e - emitter signal plus noise current

i_L - total load current

i_{nb} - transistor base-emitter shot noise current

i_{nd} - diode shot noise current

i_{nt} - thermal or Johnson noise current in a resistor

i_{st} - total diode current

K - Kelvin

K - prefix indicating x1000

k - Boltzmann's Constant (1.38×10^{-23} Joules per degree Kelvin)

ℓ - distance from film to analyzer

M_L - longitudinal or easy-axis magnetization

M_S - saturation magnetization

N - total noise current

NOMENCLATURE (Con't.)

Ni - nickel

oe - oersteds

oer - oersteds

P - photo-electric conversion efficiency (amps/watt)

p - component of light with its electric vector in the plane of incidence

$p(\alpha)$ - probability density of α

Q - symbol for transistor

q - electron charge (1.6×10^{-19} coulombs)

R_E - resistance connected to the emitter

RC - resistance-capacitance

r_b - base spreading resistance

r_e - common-emitter junction resistance

S - signal current

s - component of light with its electric vector perpendicular to the plane of incidence

T - kelvin degrees

t - light transmission coefficient of combined analyzer and lens

v - volts

W_d - incident light power onto photodector

W_o - total light power from the light source

W_r - reflected light power from the film

ΔW - change of incident light power onto photodector

α - angle of incidence of light (Ch. 3)

α - angle of field deviation from the average hard axis direction

α_1 - local easy axis deviation from the average easy axis direction

α_{90} - field angle necessary to produce 90% of saturation magnetization

β - common emitter current gain

σ - standard deviation

ϕ - Kerr angle

μ - prefix indicating micro ($x10^{-6}$)

θ - analyzer angle

χ_L - longitudinal susceptibility

ω - analyzer aperture

Investigation of the Use of the Kerr Magneto-optic Effect for the Measurement of Magnetic Fields

R. B. Yarbrough F. S. Greene, Jr.

INTRODUCTION

The use of magnetic films in a magneto-optic field detector, using a cross-field pumping scheme was discussed in the previous report*. The present report concerns the results of the continued investigation, including theoretical consideration of sensitivity and resolution. The measurement system is described and experimental results are reported.

The sensitivity of the system is ultimately dependent on the so-called "longitudinal permeability" or "longitudinal susceptibility" of the magnetic film. The longitudinal susceptibility χ_L, is related to the easy-axis dispersion in chapter 1. This development is a first-order approximation based on the gross behavior of magnetic films, and which does not take into account any dispersion of anisotropy. The calculations are statistical and assume approximately normal distribution of the dispersion of easy-axes.

In chapter 2 the system resolution is determined to be limited by the shot noise in the photodetector and the first stage of amplification. This result is verified by system measurements described in chapter 3.

*"An investigation of the use of Faraday Rotation for the Measurement of Magnetic Fields", Final Report, NASA/Ames Order A-7237A, 16 April 1968, (STAR: CR 73259) R. B. Yarbrough, F. S. Greene, Jr.

Chapter 3 gives a complete description of the measurement system, including analytical and statistical models for the various parts. Chapter 4 describes the experimental conditions and presents the results. The appendices concern the theoretical background of several formulations of chapter 3.

The work herein reported is limited to the use of the Kerr Longitudinal magneto-optic effect. Some possible means of improving the resolution of the Kerr system are discussed at the end of chapter 2, which indicate that resolution on the order of 10^{-5} oersteds is quite possible. It has been previously indicated+ that there is little difference in sensitivity between the Faraday magneto-optic effect and the Kerr longitudinal magneto-optic effect. However, because of the relatively poor contrast of the Kerr effect, as compared with the Faraday effect, better resolution may be obtainable with the Faraday effect. This possibility remains to be investigated. Furthermore, schemes for triaxial measurements remain to be investigated.

+ op. cit.

1.0 DETECTION SENSITIVITY AS A FUNCTION OF DISPERSION

In a magnetic thin film there is an "easy axis" (e.a.) which is the direction of the average remnant magnetization. Various measurements+ can be used to verify that, in any practical film, the local easy axis varies in direction from the average

A perfect film, i.e. one with no dispersion of the easy axis, would provide an infinitely sensitive detector in a field nulling magnetometer if it were used with cross-field pumping as described in CR 73259.* A film with dispersion of the easy axis will have finite sensitivity which is limited by the dispersion. The gross parameter which is affected by the dispersion is the so-called longitudinal susceptibility.

The longitudinal susceptibility (χ_L) is defined by the ratio of the net easy axis magnetization (M_L) to the easy axis magnetic field intensity (H_L) when the film is first saturated in the hard axis (i.e. the axis perpendicular to the average easy axis, lying also in the plane of the film) and then relaxed so that only the easy axis field remains.

$$M_L = \chi_L H_L \tag{1.1}$$

+ F. B. Humphrey, J.A.P., V. 38, No. 3, 1520-1527, 1 March, 1967.

* CR 73259: "An investigation of the use of Faraday Rotation for the Measurement of Magnetic Fields," R. B. Yarbrough and F. S. Greene, Jr., 16 April, 1968.

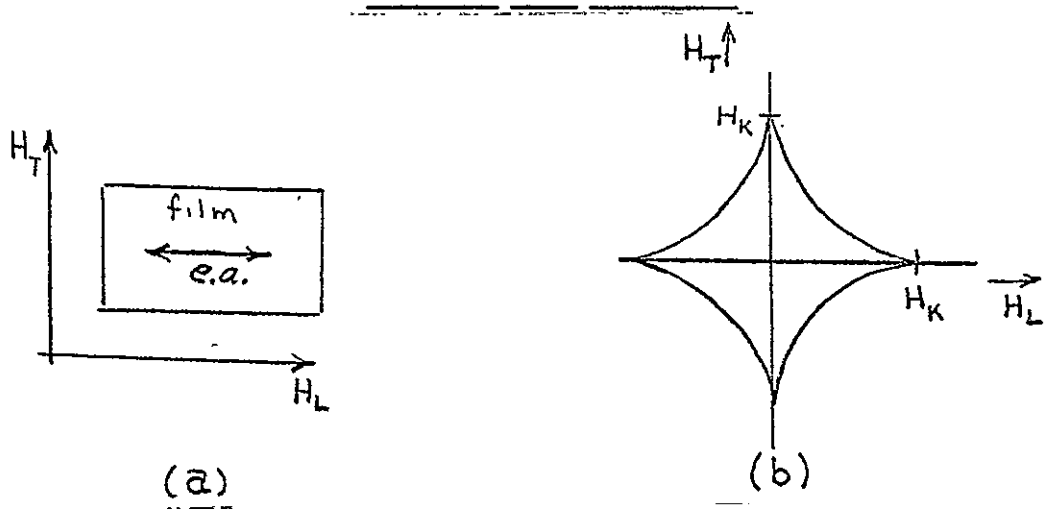

Figure 1.1(a). Film showing directions of easy axis (e.a.), Easy axis field (H_L) and hard axis field (H_T).
(b) Switching astroid for single domain particle, used as a model for ideal film.

The direction of magnetization for a single domain particle (or an ideal film) can be determined from the switching astroid. The relationship between the direction of magnetization and the applied field is as follows: On the field plane, with axes H_L and H_T, the magnetic field is plotted. The magnetization then must lie tangent to the astroid, in the upper half plan when the field is in the upper half plane, and passing through the field point. For instance, if the e.a. field H_L is zero, and $H_L > H_K$ (the anisotropy field) the magnetization is in the direction of the hard axis. If a positive H_L is then added, the direction of magnetization is in the first quadrant direction as indicated in fig. 1.2a. When the hard axis field is removed the magnetization returns to the easy axis direction as indicated in fig. 1.2b.

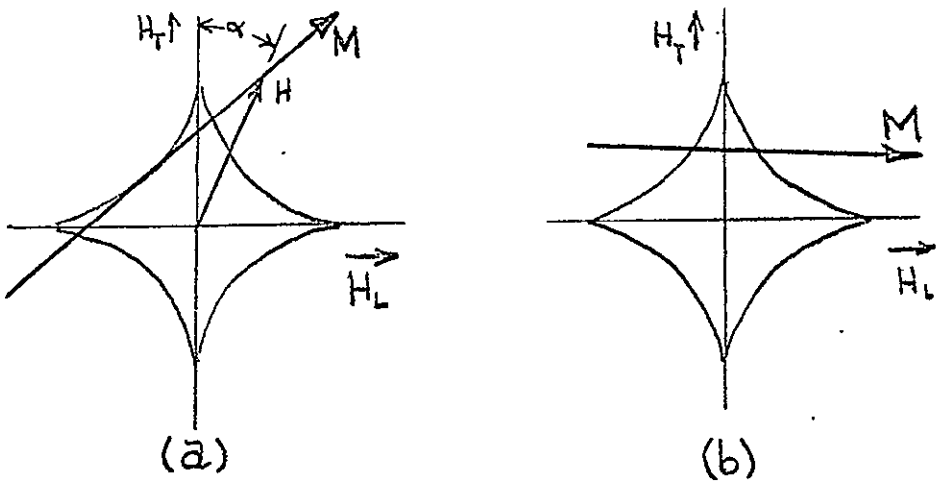

Figure 1.2(a) Direction of magnetization with $H_T > H_K$ and $H_L > 0$.
(b) Direction of magnetization after hard axis field (H_T) is relaxed.

In an actual film there is a dispersion of local easy axes about the average easy axis, and dispersion of the anisotropy field H_K about its average value. The measurements of these two dispersions can be made more or less independently. For measurement of magnitude dispersion a torque magnetometer is used* and angle measurements are usually done using Crowther's method.† While there are effects on the longitudinal susceptibility due to both dispersions, the angle dispersion is of greatest interest in this report.

While the angular dispersion of the easy axis is the term which is discussed, the effect on the longitudinal susceptibility is directly traceable to the corresponding dispersion of the local transverse or hard axis and the tilting of the local switching astroid. However, because the hard axis is

---

* R. Hasegawa, S. Uchiyama and Y. Sakaki, Journal of Applied Physics, Japan 3, 671 (1961).

†T. S. Crowther, MIT Lincoln Lab Report 51-2, March 30, 1960 (ASTIA 255697).

always 90 degrees from the easy axis, and the astroid is defined in terms of the two axes, the angular dispersion is as easily associated with one of the axes as the other. In order to be consistent with general useage, we shall then speak of the easy axis dispersion with the understanding that it actually applies to the hard axis.

Figure 1.3 shows the average axes and astroid with solid curves and a local set of axes and astroid in the dashed lines. It can be seen that in order to switch

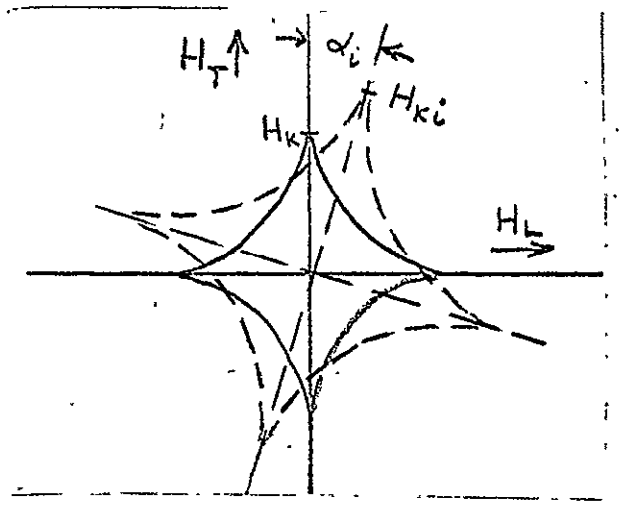

Figure 1.3 A local astroid with respect to the average.

the magnetization of the local point i to the positive average H_L direction, the total field must have an angle greater than α_i and be greater in magnitude than H_{Ki}. If the total field has magnitude greater than H_{Ki} and the angle is less than α_i, the magnetization at this point will, in the absence of interractions from nearly magnetization, tend toward the negative H_L direction when the hard axis component of field (H_T) is removed. A measure of the dispersion of the easy axis which is commonly used is the angle of applied field, as measured from the hard axis, which is necessary to cause 90% of the maximum magnetization to lie in the positive H_L direction

when H_K is removed. This angle is commonly called α_{90}. When the conditions $H_L / H_T = \tan \alpha_{90}$ have been applied, the final condition of the film is that 95% of the magnetization has been switched to the $+H_L$ direction and 5% has been switched to the $-H_L$ direction, so that the remnant magnetization is 90% of the maximum. In this procedure, the dispersion of the anisotropy is only mildly contaminating of the measurement at remnance.

Clearly, the range of α is from -90 to +90 degrees. The value of α_{90} is typically less than 10 degrees in films that were made in a constant magnetic field.

Let us consider that α_i has a symmetrical probability density about zero degrees, so that

$$\int_{-90^o}^{90^o} p(\alpha_i)d\alpha = 1 \qquad (1.2)$$

where $p(\alpha)$ is the probability density function of α_i. Then it is possible to describe the remnant magnetization in terms of this probability density function and the direction of the applied field:

$$M_L = M_S \int_{-90}^{\tan^{-1}(H_L/H_T)} p(\alpha_i)d\alpha - M_S \int_{\tan^{-1}(H_L/H_T)}^{+90} p(\alpha_i)d\alpha \qquad (1.3)$$

where the first term on the right-hand side of eq. 1.3 corresponds to the fraction of magnetization which switched to the $+H_L$ direction and the second term corresponds to the fraction which switched to the $-H_L$ direction when H_T was relaxed. M_S is the saturation value of magnetization or the maximum remnant value.

As the probability from -90 to 0 degrees is identical to the probability from 0 to +90 degrees, by symmetry, eq. 1.3 can be rewritten:

$$M_L = 2M_S \int_0^{\tan^{-1} \frac{H_L}{H_T}} p(\alpha_i)d\alpha \qquad (1.4)$$

Crowther* has assumed a normal distribution of α_i . It is noted that α_{90} is typically less than 10^0. Using this basis, it is equally valid to assume that $\tan \alpha_i$ will have a normal distribution and that α_i (radians) = $\tan \alpha_i$. In this case, eq. 1.4 is written:

$$M_L = 2M_S \int_0^{H_L/H_T} p(\tan \alpha_i)d \tan \alpha \qquad (1.5)$$

where $P(\tan \alpha_i)$ can be written at the 90% value

$$M_L = .9M_S = 2M_S \int_0^{\tan \alpha_{90}} p(\tan \alpha_i)d \tan \alpha \qquad (1.6)$$

For the assumed normal distribution, let $X = \tan \alpha_i$

$$p(X) = \frac{1}{\sqrt{2\pi}\,\sigma} e^{-\frac{1}{2}\frac{X^2}{\sigma^2}} \qquad (1.7)$$

when this value is placed in eq. 1.6,

$$2 \int_0^{\tan \alpha_{90}} p(X)dx = .9 \qquad (1.8)$$

---

*Ibid.

which is satisfied when $\sigma = .51 \tan \alpha_{90}$

or $\tan \alpha_{90} = 1.96\sigma$

In order to obtain general information under the assumptions made, it is necessary to cast eq. 1.5 in a more useful form:

$$M_L = \frac{2M_S}{\sqrt{2\pi}} \int_0^{H_L/\sigma H_T} e^{x^2/2} \, dx \tag{1.9}$$

where $x = \frac{\tan \alpha}{\sigma}$

The susceptibility is defined as $\frac{\partial M_L}{\partial H_L}$. Taking the derivative of an integral with respect to the upper limit:

$$\chi_L = \frac{dM_L}{dH_L} = \frac{2M_S}{\sqrt{2\pi}} \frac{1}{\sigma H_T} e^{\frac{1}{2}\left[\frac{H_L}{\sigma H_T}\right]^2} \tag{1.10}$$

so that the initial susceptibility is

$$\chi_{LO} = \sqrt{\frac{2}{\pi}} \frac{1.96}{\tan \alpha_{90}} \frac{M_S}{H_T} = \frac{1.56}{\tan \alpha_{90}} \frac{M_S}{H_T} \tag{1.11}$$

A normalized plot of M_L vs H_L is shown in fig. 1.5. It is to be noted that this development is independent of the dispersion of H_K provided that H_T is larger than the largest value of H_K.

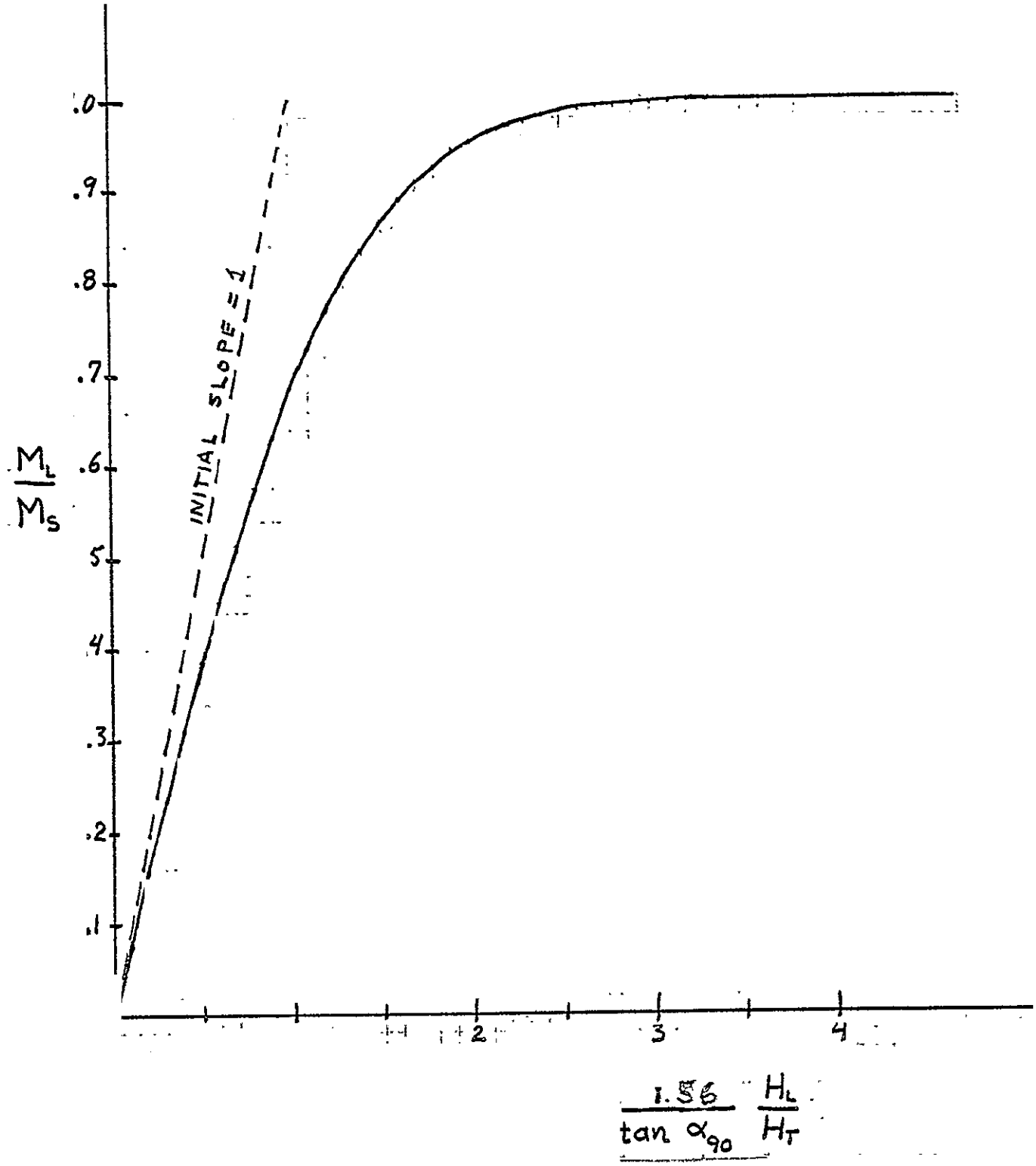

Figure 1.5. Normalized plot of M_S vs. H_L with cross-field pumping greater than H_K.

2. LIMITATIONS RELATED TO LIGHT INTENSITY

There are many sources of noise in the system, but the point where the noise is most determinative of resolution is where the light signal is converted to an electrical signal. The system chosen for the detection scheme is a photodiode connected to the base of a high gain, low noise transistor. While the photodiode is slightly less efficient than a photomultiplier tube, its matching to the transistor gives this system advantages over a photomultiplier tube, one of which is the lower operating voltage.

The photodiode is chosen over a phototransistor because the shot noise generated is very nearly $2qI\Delta f$ in the photodiode as well as the low noise transistor, while phototransistors tend to be much noisier.

The low noise transistor can be connected in either in the common emitte (C.E.) or the common collector (C.C.) configuration as indicated in fig. 2.1 For noise analysis the noise sources within the photodiode and transistor

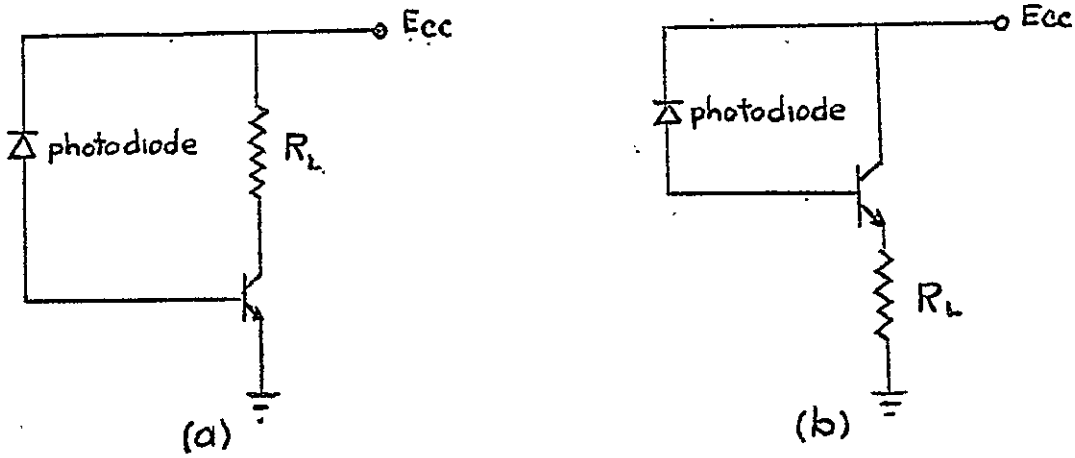

FIGURE 2.1 PHOTODETECTION INPUT STAGE: (a) CE; (b) C.C.

are shown in figure 2.2. As the photodiode is essentially a current source, the combined equivalent circuit is as shown in figure 2.2(c). The noise source

due to r_b and r_b can be neglected because they are in series with the photodiode which is a current source. As the transistor is current driven

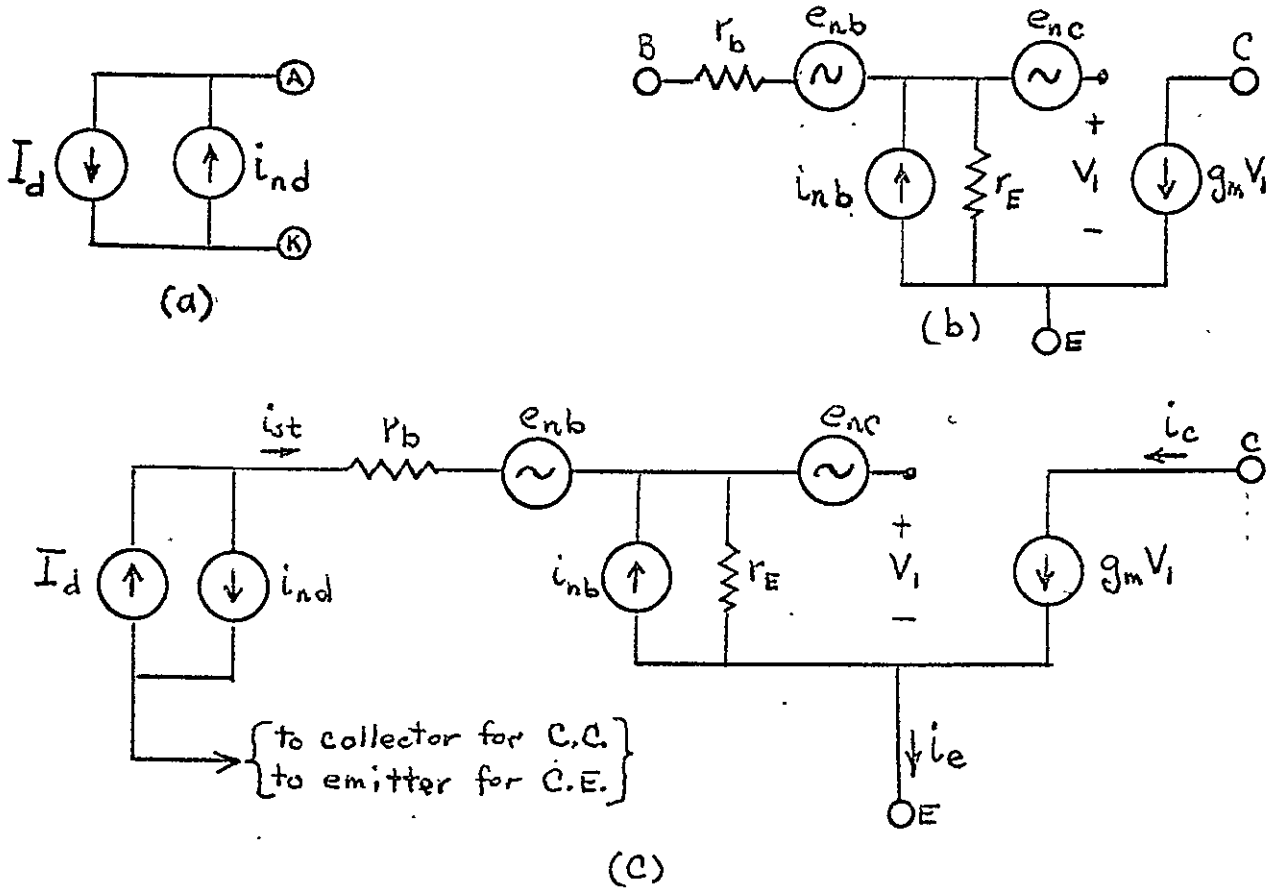

FIGURE 2.2: EQUIVALENT CIRCUITS INCLUDING NOISE SOURCES:
(a) Photodiode; (b) Transistor; (c) Photodiode with Transistor.

it is possible to determine i_E and i_C for either C.C. or C.E. connection:

$$i_c = g_m [e_{nc} + r_E (i_s + i_{nd} + i_{nb})] \tag{2.1}$$

$$i_e = i_{st} + i_{nd} + i_c \tag{2.2}$$

The noise sources in this circuit are to be understood as shot noise and flicker noise. The flicker noise is important at low frequencies, taking on a frequency dependence of $1/f$. For currently available devices the flicker noise corner frequency is well below 500 Hz, and so will not be important in this application.

The shot noise sources have values* dependent on the d.c. current values:

$$\bar{i}_{nd}^2 = 2qI_d\Delta f \tag{2.3}$$

$$\bar{i}_{nb}^2 = 2qI_b\Delta f \tag{2.4}$$

$$\bar{e}_{nc}^2 = 2qI_c\Delta f/g_m^2 \tag{2.5}$$

where $q = 1.6 \times 10^{-19}$

Δf = amplifier bandwidth

The voltage noise source e_{nc} is due to the collector shot noise but is referred back to the base.

CIRCUIT NOISE SOURCES

There are two sources of noise outside the semiconductors, the thermal noise of the load resistor and power supply noise. The power supply noise can be greatly attenuated by using both filtering and common mode rejection techniques. If this noise is predominantly ripple, the use of common mode rejection techniques (i.e. differential amplifiers) can easily achieve 60 d.b. of attenuation, which will reduce most such noise well below other sources. The power supply noise can be greatly diminished by use of the C.C. connection, also, because the drive is a current source, slightly greater gain is achieved using the C.C. connection.

In the C.C. connection, only the thermal noise is of significance. The thermal or Johnson noise has an equivalent noise current source in parallel with

* A. Vander Ziel, ELECTRONICS, Allyn and Bacon, 1966, Ch. 23.

the resistance:

$$\bar{i}_{nt}^2 = 4kT\Delta f/R \qquad (2.6)$$

SIGNAL PLUS NOISE

The total output current, including all noise sources can be calculated:

$$i_L = i_E + i_{nt} \qquad (2.7)$$

$$i_L = (1+g_m r_E)\, i_s + (1+g_m r_E)\, i_{nd} + g_m e_{nc} + g_m r_E\, i_{nb} + i_{nt} \qquad (2.8)$$

As the signals are independent, they can be added only by the Root mean squared method. The signal is the first term $(1+g_m r_E)i_s$ and the remaining terms are noise, and as $\beta = g_m r_E$:

$$N^2 = (1+\beta)^2(2qI_d\Delta f) + g_m^2(2qI_c\Delta f/g_m^2) + \beta^2 2qI_b\, f + 4kT\Delta f/R \qquad (2.9)$$

As $I_d = I_b$ and $I_c \cong \beta I_b$, eq. 2.9 can be written:

$$N^2 = 2qI_d\Delta f(2\beta^2 + 3\beta + 1) + 4kT\Delta f/R \qquad (2.10)$$

with β on the order of 200:

$$N^2 \cong (\beta^2 qI_d + kT/R)4\Delta f \qquad (2.11)$$

Assuming a load resistance on the order of 10K ohms to give a good match to the amplifier; and a bandwidth of 60 Hz:

$$N^2 = 1.536 \times 10^{-12}\ \ Id + 9.6 \times 10^{-27} \qquad (2.12)$$

It can therefore be seen that the shot noise predominates and the thermal noise can be neglected, if Id is of any reasonable value. The signal to noise ratio

is then approximated by:

$$\frac{S}{N} = \frac{i_s}{2\sqrt{qI_d\Delta f}} \tag{2.13}$$

which differs from the signal to noise ratio of the photodiode alone by the factor of the square root of two. This figure is identical to that which could be expected from a low noise phototransistor if it were available.

RELATION TO LIGHT INTENSITY

The average value of the photodiode current is dependent on the ambient light intensity upon the photodiode:

$$I_d = PW_d \tag{2.14}$$

where P is the conversion efficiency (Amps/Watt) W_d = incident light (watts) on photodiode.

The signal has the same dependence on the light intensity variation:

$$I_s = P\Delta W_d \tag{2.15}$$

The signal to noise ratio can then be written:

$$\frac{S}{N} = \frac{\sqrt{P\Delta W_d}}{\sqrt{4q\Delta f W_d}} \tag{2.16}$$

Based on the light power emitted from the light source (see section 3 below) the ambient light incident on the photodiode is:

$$W_d = .035W_o \sin^2\theta \tag{2.17}$$

where W_o = total light power from the light source

θ = angle of the analyzer from minimum transmittance.

The maximum change in light power is obtained by first saturating the film in one easy direction and then reversing the field to saturate in the opposite easy direction. The minimum change in field is then $2H_{sat}$. The change in light power in this situation is:

$$\Delta W_{max} = .00875\ W_o \sin 2\phi \sin 2\theta \tag{2.18}$$

where ϕ = Kerr effect angle = 5 minutes

then:

$$\frac{\Delta W_{max}}{\sqrt{W}} = .0935\sqrt{W_o} \sin 2\phi \cos \theta \tag{2.19}$$

The maximum signal to noise ratio is then:

$$(S/N)_{max} = \frac{.0935\sqrt{PW_o} \sin 2\phi \cos \theta}{\sqrt{4q\Delta f}} \tag{2.20}$$

The minimum signal which can be resolved is taken as that which gives a signal to noise ratio of one:

$$(S/N)_{min} = 1 = \frac{\sqrt{P\Delta W}_{min}}{\sqrt{4q\Delta f W}} = \frac{\Delta W_{min}}{\Delta W_{max}} \left(\frac{S}{N}\right)_{max} \tag{2.21}$$

The minimum field which can be resolved then is proportional to the minimum light signal:

$$H_{min} = \frac{2\Delta W_{min} H_{sat}}{\Delta W_{max}} = \frac{2H_{sat}}{(S/N)_{max}} \tag{2.22}$$

Then

$$H_{min} = \frac{\sqrt{4q\Delta f}\ H_{sat}}{.187\sqrt{PW_o} \sin 2\phi \cos \theta} \tag{2.23}$$

or

$$H_{min} = \frac{.114 \times 10^{-5} H_{sat}}{\sqrt{PW_o}} \qquad (2.24)$$

The radiant sensitivity is listed as 1.6 microamperes per milliwatt per square centimeter referred to the base of the Fairchild FPT 100 phototransistor. This number is obtained by using 5 milliwatts per square centimeter at a color temperature of 2870 ^{o}K, which corresponds to a wavelength of about 0.45 microns. The luminous efficiency of the photodiode is about 22% at this color temperature. The Zenon arc has its output concentrated in the band between .8 and 1 micron wavelengths where the luminous efficiency is on the order of 95%. Then a fourfold increase of radiant sensitivity can be expected. With an area of 1.8 mm^2, the value of P is then .115 microamps per milliwatt.

The value of H_{sat} is measured to be .05 oersteds. The dispersion curve Fig. 1.5 indicates that for fields near zero, the linear extrapolation of the initial slope indicates a reduction by a factor of .4 from this value, so that the value of H_{sat} should be taken as .02.

The emitted light power, W_o, is conservatively estimated to be .004 watts. With these values:

$$H_{min} = \frac{(.114 \times 10^{-5})(2 \times 10^{-2})}{(.115 \times 10^{-3} \times .4 \times 10^{-2})^{1/2}} = 3.36 \times 10^{-5} \text{ oersteds}$$

This value can be improved by several means:

(1) A differential scheme will improve S/N by a factor of the square root of two.

(2) H_{min} will decrease as the square root of the light power.

(3) H_{min} will decrease as the square root of the band width decreases.

3.0 MAGNETO-OPTIC INSTRUMENT

3.1 Longitudinal Kerr magneto-optic effect.

(a) Magneto-optic effects - general description

There are two types of magneto-optic effects, Faraday effect and Kerr effect.[1] The Faraday effect involves the change in polarization or intensity of plane polarized light transmitted through a magnetized medium. The Kerr effect involves the change in polarization or in intensity of plane polarized light reflected from the surface of a magnetized medium. The longitudinal Kerr effect is one of a family of three Kerr effects that are classified according to the direction of the magnetization with respect to the plane of incidence and to the reflecting surface. The other two are the polar and transverse effects. Both the Faraday and Kerr effects occur in ferromagnetic media; however, the Faraday effect also occurs in ferrimagnetic and paramagnetic media. The Kerr effects occurs only in media with an absorption index so that the complete index of refraction is complex. Since the Kerr effect depends on having a smooth specular reflecting surface for the magnetic media, in many cases it is difficult to detect. Both the Faraday and Kerr effects are strong in magnetic films of iron, nickel, cobalt, and permalloy. For transparent films the Faraday effect can be used, whereas for opaque films the Kerr effect is necessary. In addition, there is a Kerr electro-optic effect that is not related to the Kerr magneto-optic effect, and the two should not be confused. All references to the Kerr effect will automatically mean the longitudinal magneto-optic effect.

(b) Longitudinal Kerr magneto-optic effect

The longitudinal Kerr effect can be described as follows. A reflecting ferromagnetic sample is magnetized in a direction that is both parallel to the plane of incidence and the surface of the material as shown in Figure 3.1. If plane

polarized light with its electric vector perpendicular to the plane of incidence, E_{si} , (s light) is reflected obliquely from the magnetized surface, a s component appears in the reflected beam, E_{sr} , as in the case of ordinary metallic reflections. In addition, because of the magnetization of the ferromagnetic sample, a small p component, E_{pr}, appears in the reflected beam. Since, in general, E_{pr} is out of phase with E_{sr}, the total reflected light is elliptically polarized with the major axis of the ellipse rotated off of the s axis. These polarization effects are called the Kerr ellipticity and rotation. As also shown in Figure 3.1, a reversal in the magnetization direction produces a sign reversal in E_{pr}, so that the major axis of the ellipse is symmetrically rotated to the other side of the s axis. The sign of the ellipticity also reverses. A similar effect occurrs for the incident light plane polarized with the electric vector parallel to the plane of incidence (p light). In this case, the Kerr ellipticity and rotation take place around the p axis. The longitudinal Kerr effect disappears at normal incidence.

The size of the Kerr effect depends on the saturation magnetization of the ferromagnetic sample, the wave length of the incident light, the angle of incidence, and the relative size and phase of the p and s metallic reflection coefficients.

For all of the experiments on metal films, the incident beam is s polarized to obtain the longitudinal Kerr effect without any transverse Kerr effect components. Therefore, if the magnetic media is magnetized perpendicular to the plane of incidence there is no Kerr signal. This eliminates any magneto-optic signal that would appear as noise for the longitudinal Kerr effect signal.

Because the polarization of the reflected beam is the vector sum of the ordinary metallic reflection component and the Kerr component, the polarization angle will decrease with increasing light wavelength since the Kerr reflection coefficient is reduced while the metallic reflection coefficient is increased.

The experimental techniques for using the longitudinal Kerr effect for domain

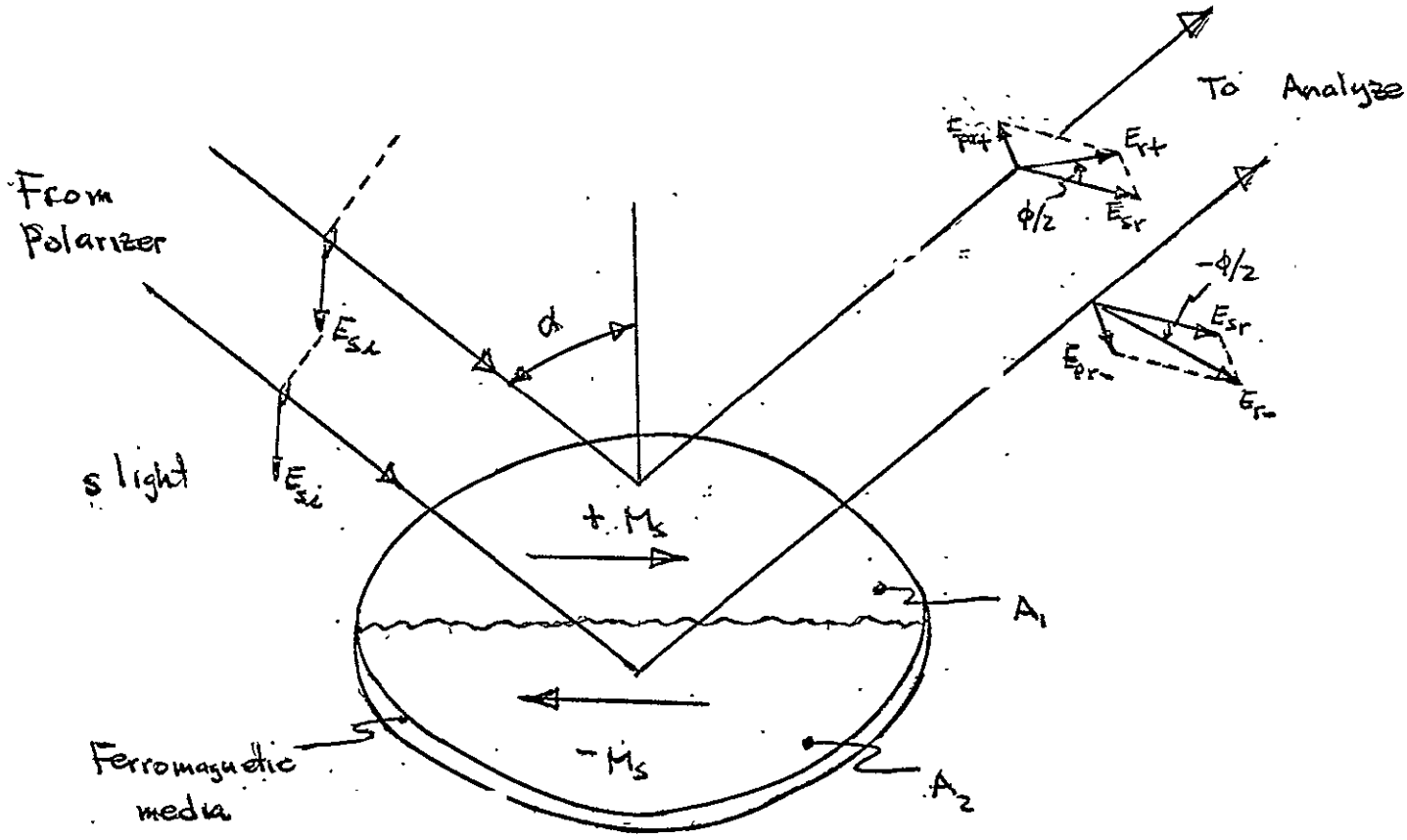

$E_{(i)}$ - light electric vector

M_s - saturation magnetization

α - angle of incidence

Φ - Kerr polarization angle

Fig 3.1 Longitudinal Kerr Magneto-optic effect

observation were developed mainly by Fowler and Fryer.[4] The sensitivity limitations of the Kerr magneto-optic technique have been discussed by a number of authors.[3-6] Theoretical descriptions of the Kerr magneto-optic effect for magnetic films have been given by Lissberger,[7] Robinson,[8] and Yoshino and Tanaka.[9] These results are used in the design and construction of the magneto-optic instrument to be discussed in detail later.

3.2 Magneto-optic signal and sensitivity limitations

(a) Magneto-optic signal

The electric field vector of the reflected light, E_r, is the vector sum of $E_{pr(\pm)}$ and E_{sr}. The intensity of the light reflected from the magnetic media can be written as

$$I_o \sim E_r E_r^* \tag{3.1}$$

where E_r^* is the complex conjugate of E_r. If another polarizer (the analyzer) is put in the path of the reflected light from a magnetized sample, then the light intensity transmitted through the analyzer is given by

$$I_D = I_o t(\sin^2\theta + \varepsilon) \tag{3.2}$$

where θ is the angle the analyzer is rotated from its position of minimum transmission, t is the transmission coefficient of the analyzer and focusing lens, and ε is the extinction factor at minimum transmission. If the magnetic media is completely magnetized in the opposite direction, then the light transmitted by the analyzer is given by

$$I_D = I_o t[\sin^2(\theta + \phi) + \varepsilon] \tag{3.3}$$

where ϕ is the Kerr polarization angle. Therefore, the longitudinal Kerr effect can be used to measure the both the direction and amplitude of the longitudinal component of the magnetization by detecting the light intensity change due to the

Kerr angle, ϕ .

In the case where the magnetic media consist of domains magnetized in opposite directions, then the area of these domains have to be included in the magneto-optic signal. For the domain areas, A_1 and A_2, shown in Figure 3.1 the power of the reflected light that is transmitted through the analyzer can be written as

$$W_r = I_o t[A_1 \sin^2(\theta+\phi) + A_2 \sin^2 \theta] \tag{3.4}$$

Where the extinction factor, ε, has been omitted since it is negligible for the polarizers used here at the usual operating value for θ where magneto-optic signal is important. The magneto-optic signal that includes both the difference in domain area and magnetization direction and amplitude can be written as

$$\Delta W = I_o t\{[A_1 \sin^2(\theta+\phi) + A_2 \sin^2 \theta] - \frac{A_T}{2}[\sin^2(\theta+\phi) + \sin^2 \theta]\} \tag{3.5}$$

where $A_1 + A_2 = A_T$ - total illuminated area and ΔW_m is zero when $A_1 = A_2 = A_T/2$. Let $A_1 - A_2 = \Delta A$ - differential domain area. Then the magneto-optic signal power can be written as

$$\Delta W = I_o t \frac{\Delta A}{2} [\sin^2 (\theta+\phi) - \sin^2 \theta] \tag{3.6}$$

Since the Kerr angle, ϕ , is on the order of a few milliradians and signal and not contrast is important, θ is set so that $\theta >> \phi$. Under these conditions

$$\Delta W = I_o t \frac{\Delta A}{2} \phi \sin 2\theta \tag{3.7}$$

Thus the magneto-optic signal is directly proportional to both the differential domain area and the magnetization. Therefore, a variation in the differential domain area influences the magneto-optic signal in the same way as a magnetization change. However, the physical reasons for the signal change are different. The signal due to the differential domain area comes from more or less light transmitted

through the analyzer as the size of the area with the maximum, but fixed, Kerr angle, ϕ , is increased or decreased; whereas, the signal due to a magnetization change comes from the variation in the Kerr polarization angle of the reflected light. Unfortunately, in the magneto-optic signal these different variations can not be separated.

The average light power reading the photodetector is given by Eq. (3.4). This determines the quiescent bias current in the photodetector since it is operated otherwise in the cutoff mode.

(b) Noise

Although the magnitude of the magnetic signal has been determined, the maximum sensitivity of the Kerr instrument cannot be predicted until the noise sources have been considered. The major sources of noise are: the shot and thermal noise in the photodetector; the optical noise due to surface imperfections such as pinholes, dust and scratches; the light level fluctuations due to arc instability and slight changes in the alignment of the optical system during the readout process.

(c) Optical noise sources

The important optical noise sources for this Kerr instrument are surface imperfections such as dust, pinholes, and scratches and arc instabilities. By using parallel light, the ellipticity caused by metallic reflection of non-p or non-s light is avoided. Since no lens are placed between the polarizer and analyzer, lens depolarization and Faraday effects are also avoided.

The pinholes and dust scatter the light roughly as if they were pinholes in the path of a plane wave. Thus the diffracted light is scattered with a cone angle, B, of the order of $B \simeq \lambda/d$ where λ is the wavelength of light and d is the size of the pinhole. Although the incident is plane polarized, the scattered light is essentially completely depolarized. Therefore, the scattered light is independent of the analyzer angle θ . Since the magnetic signal, Eq. (3.7) depends

on θ , the signal to noise ratio due to surface imperfections can be increased by increasing θ . Thus, the analyzer angle is set to its largest value possible, consistent with the signal to noise ratio of other noise sources. Since a parallel beam is being used, most of the scattered rays will not be collected by the analyzer provided $\omega/\ell << B$ where ω is the analyzer apperature and ℓ is the distance from the analyzer to the magnetic media.

The other major optical noise source, light level fluctuations, can be minimized by a differential detection scheme described by Treves.[6] This is based on the optical noise signals being common mode and the magnetic signal being a differential mode signal. A carefully selected nonpolarizing beam splitter is used to amplitude split the beam into two analyzers where one is set at $+\theta$ and the other at $-\theta$ to the minimum transmission position. The output of the two photo-detectors are fed to a difference amplifier that reduces the common mode by 60 to 80 db signals while amplifying the differential magneto-optic signal to significantly improve the signal to noise ratio. This differential detection scheme has not been used in the Kerr instrument described in this report, but will be implemented as soon as possible.

3.3 Kerr Magneto-optic instrument

(a) Detailed description of optics

The optical system used in the Kerr magneto-optic instrument is shown in Figure 3.2. The light source is a 75 watt xenon short arc lamp (Illumination Industries III 75) with a brightness of 1500 lumens and arc size of .305 x .305 mm.[2] The lamp house (Illumination Industries LH 350) contains a pyrex condenser (f = 38 mm a = 45 mm) with a collection angle of $.8\pi$ steradian at 38 mm. An additional condensing lenses (f = 126 mm, a = 40 mm) is used to obtain a parallel beam. An adjustable iris between the condensing lens is used to set the beam

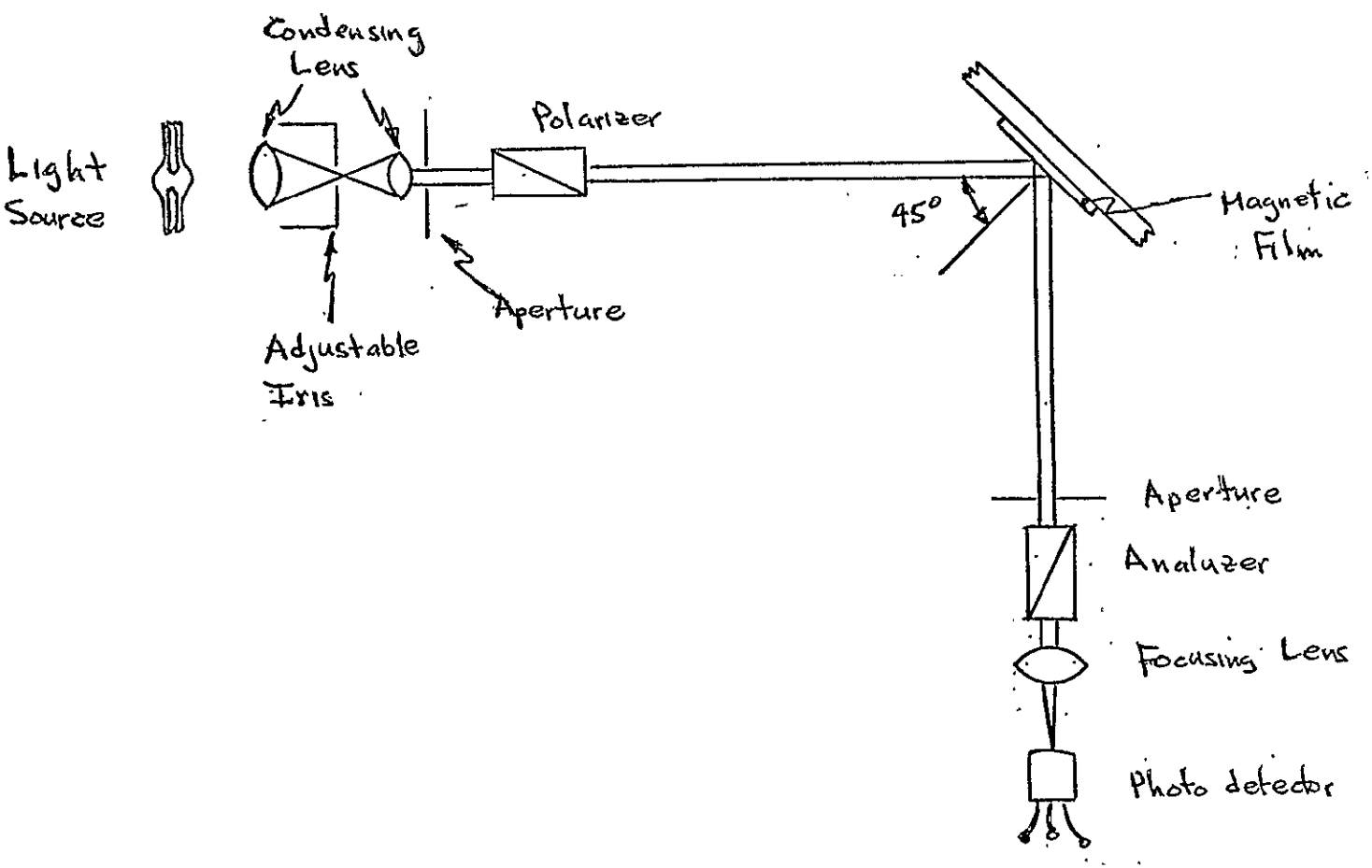

Fig. 3.2 Optical System

diameter to about 10 mm.

The parallel beam is polarized by a Glan Thompson 10 x 10 mm^2 prism which transmits about 45% of the incident unpolarized light spectrum between 4000 Å and 20,000 Å. The prisms are mounted in special micropositioners that were developed by Ampex Corporation (R. P. Hunt). With this micropositioner the angular position of the polarizer can be repeatably set to 1' of arc. The beam is reflected from the magnetic film surface into another Glan Thompson polarizing prism that is used as an analyzer. The analyzer beam is then focused onto the collector-base junction of an FPT 100 (Fairchild Semiconductor) silicon NPN phototransistor with a light to collector current conversion coefficient of 15 amp/watt for a tungsten lamp at a 2870° K color temperature. The xenon arc was chosen to match the spectral response of the FPT 100 phototransistor in the infrared region (≈ 8000Å).

The light power incident on the magnetic film surface is calculated to be 10^{-3} watts, assuming 50% lens transmission coefficients and 45% polarizer transmission coefficients.* The average light power into the phototransistor is 10^{-5} watts with a maximum magnetic signal light power of 4×10^{-8} watts.

(b) Photo detector electronics

The photo transistor emitter current, generated by the light level change due to the magnetic film switching, produces a voltage across R_e that is amplified by the low noise differential amplifier shown in Figure 3.3. The differential amplifier output is amplied by an μA 741 integrated circuit operational amplifier. Q_2 and Q_3 are biased at 10 μa of collector current so as to operate in the minimum noise figure (F < 4db) region for a source resistance of 20 kΩ. The overall amplifier gain is set to 100 by the ratio of the feedback resistors around the μA 741. The dc bias level at the input to the μA 741 is set by adjusting R_2 to compensate for the dc signal due to the average light level into the photo transistor. In this way, the μA 741 can always be biased into its linear operating region with a

* See Appendix 3

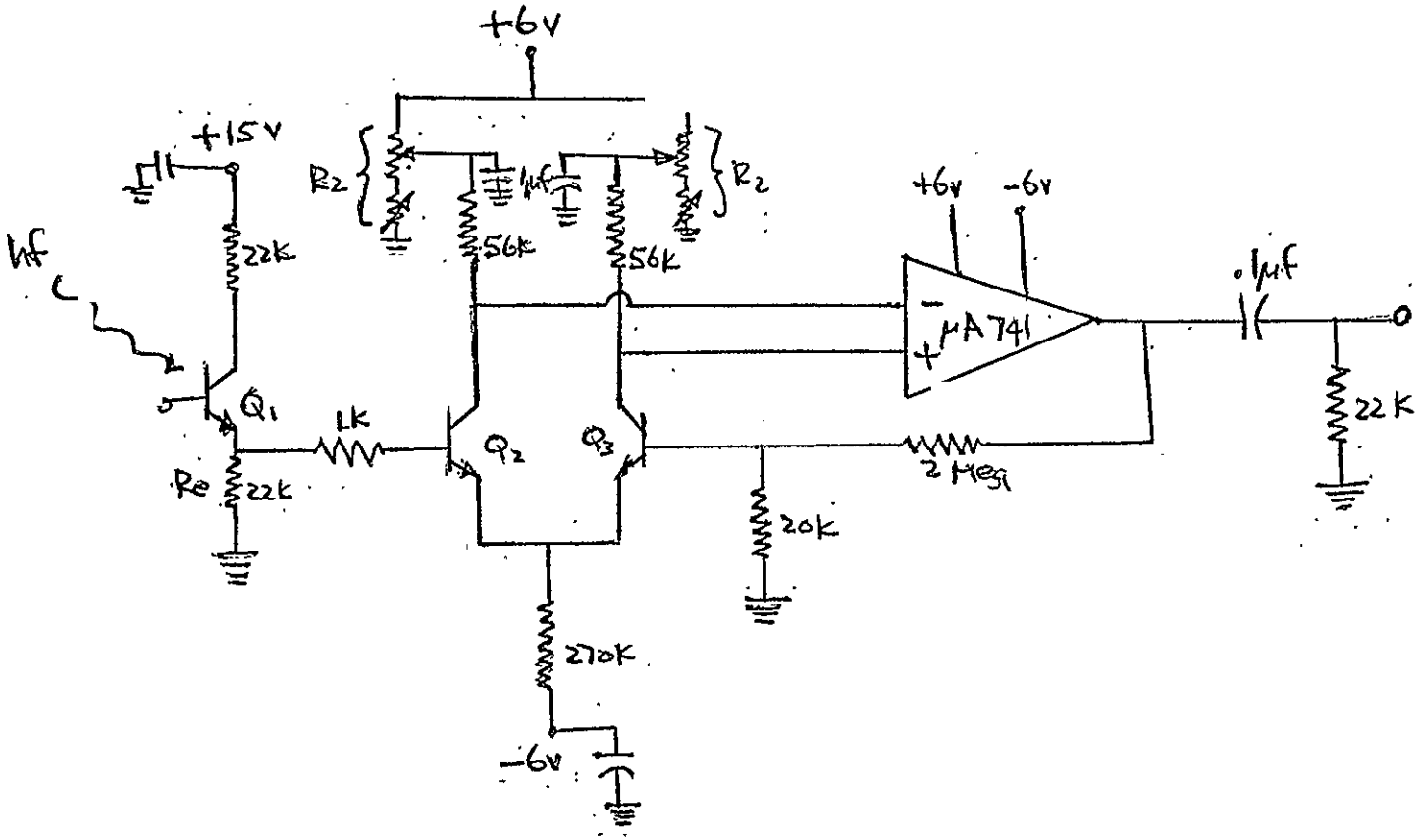

Q_1 – FPT 100

Q_2, Q_3 – FT107B (dual)

Fig 3.3 Photo detector Amplifier

minimum of common mode dc voltage. The output noise at 1000 hz bandwidth measured 1 millivolt peak to peak. This is equivalent to a 10 μ volts noise source at the amplifier input. The major source of electronic noise is shot noise in the phototransistor as indicated by the signal to noise calculations earlier. This was verified by disconnecting the phototransistor and measuring the amplifier output noise voltage. Under this condition, the output noise voltage was about .25 millivolts or an equivalent input noise voltage of 2.5 μ volts.

A wave analyzer is connected to the output of the photo detector amplifier to measure the magneto-optic signal over only a $\pm$ 30 hz bandwidth to give maximum signal to noise ratio.

(c) Field drive

The earth's field and other static fields are nulled by a triaxial set of Fanselau coils by Marshall Laboratories, Model ML 131-1, to a resolution of 10^{-5} oersted. Both static and alternating fields are provided by an orthogonal set of Helmholtz coils with the following parameters

Vertical Field Coils

Low field - 3.9 oer/amp, 36 turns, 7.25" ID

High field - 39 oer/amp, 324 turns, 7.75" ID

Horizontal Field Coils

Low field - 3.5 oer/amp, 50 turns, 10.00" ID

High field - 28 oer/amp, 424 turns, 11.00" ID

The Helmholtz coils are connected to the appropriate power source through a patch wire control box as shown in Figure 3.4. Field measurements between 1 oer and 10^{-6} oer are made with a fluxgate magnetometer by Foster Hoover Electronics, Model MF-5050. The alternating field current is supplied by a 25 watt motion picture power amplifier and static field current by Harrison Lab, 36 v, 5 amp, dc power supplies. For alternating fields, the Helmholtz coils are driven as a series

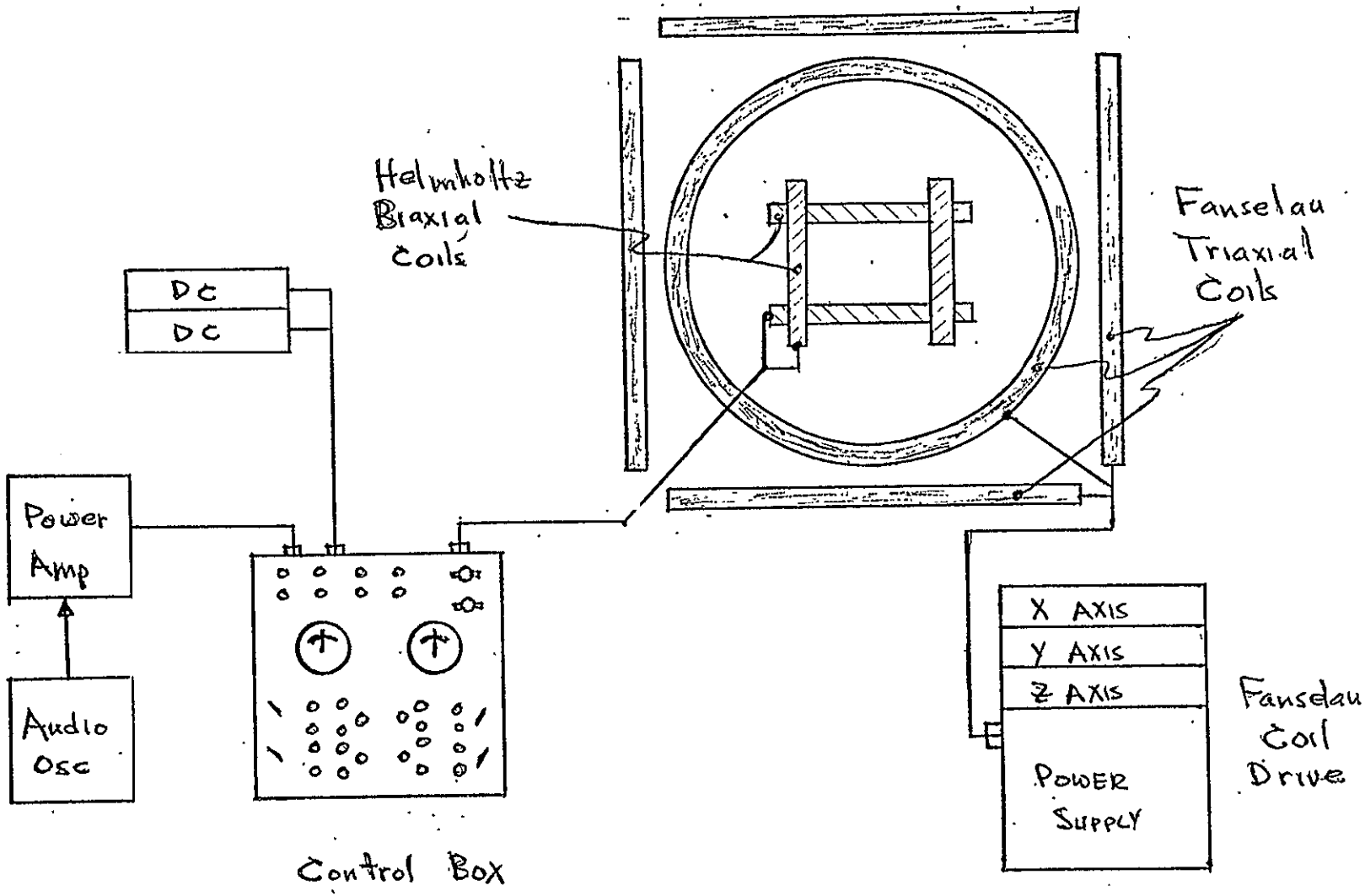

Fig. 3.4 Field Drive

resonance circuits so that the power amplifier load impedance can be controlled to be 16 ohms. The remaining coil electrical parameters along with the control box circuit diagram are included in Appendix 1. The Helmholtz coil set is mounted on a rotatable bearing plate so that the angle of incidence between the magnetic sample and light beam can be varied while maintaining a fixed field drive direction relative to the magnetic sample. This also allows for Faraday effect measurements to be readily implemented.

(d) System Operation

With the patch panel control box, the Kerr instrument can be easily connected to do many types of switching measurements. For the magnetometer measurement, the power amplifier drives the high field vertical coils to produce an alternating field in the hard direction of the magnetic film and a dc power supply is connected to the low field horizontal coils to produce a static field in the easy direction. The magnetic film sample is positioned with its average easy axis parallel to the plane of incidence of the light beam. The photo detector amplifier is connected to a narrow band ($\pm$ 30 hz) wave analyzer to obtain maximum signal to wire ratio. Also, the M-H hysteresis loop can be displayed on an oscilloscope by connecting the horizontal axis to the field monitor points of the control box and the vertical axis to the photo detector amplifier. A RC phase delay circuit delays the field input signal to match the delay of the magneto-optic signal through the photo detector amplifier. In this way, correctly phased M-H hysteresis loops are displayed on the oscilloscope.

The wave analyzer is tuned to the second harmonic of the alternating hard direction drive field to detect the magneto-optic signal produced by the easy direction static field. The second harmonic voltage versus the static easy direction field gives the magnetometer sensitivity.

4.0 Experimental Results

4.1 Magneto-optic set up

The Kerr magneto-optic instrument is set up as follows for the magnetometer measurement

Incident light polarization - S light

Angle of incidence: 45 degrees

Analyzer angle, θ : 10 degrees

Avg. light into photo detector: 10 microwatts

Analyzer distance from film, ℓ : 53.5 cm

4.2 Magnetometer measurement

The magnetic film used for the magnetometer measurements had the following properties.

Composition - 81% Ni - 19% Fe

Thickness - 1000 Å

Hk = 4.4 oer

Hc = 2.5 oer

$_{90} = 1.5^{o}$

Substrate - 1" x 1" microscope slide

The magnetic film is switched into the hard direction by a 500 hz sine wave field. The hard direction field H_T , is large enough to completely saturate the film in the hard direction so that $H_T \geq H_K$. The hard direction of the film is experimentally aligned with H_T by observing the crossed field M-H hysteresis loop (M_L vs H_T) and positioning for zero output. The static easy direction fields are nulled to $< 10^{-5}$ oer by the Fanselau coils as measured by the Foster-Hoover, model 5005, magnetometer. Known values of easy direction fields are applied through the Helmholtz coils with the dc power supplies. The resulting net easy direction (longitudinal) magnetization produces a magneto-optic signal

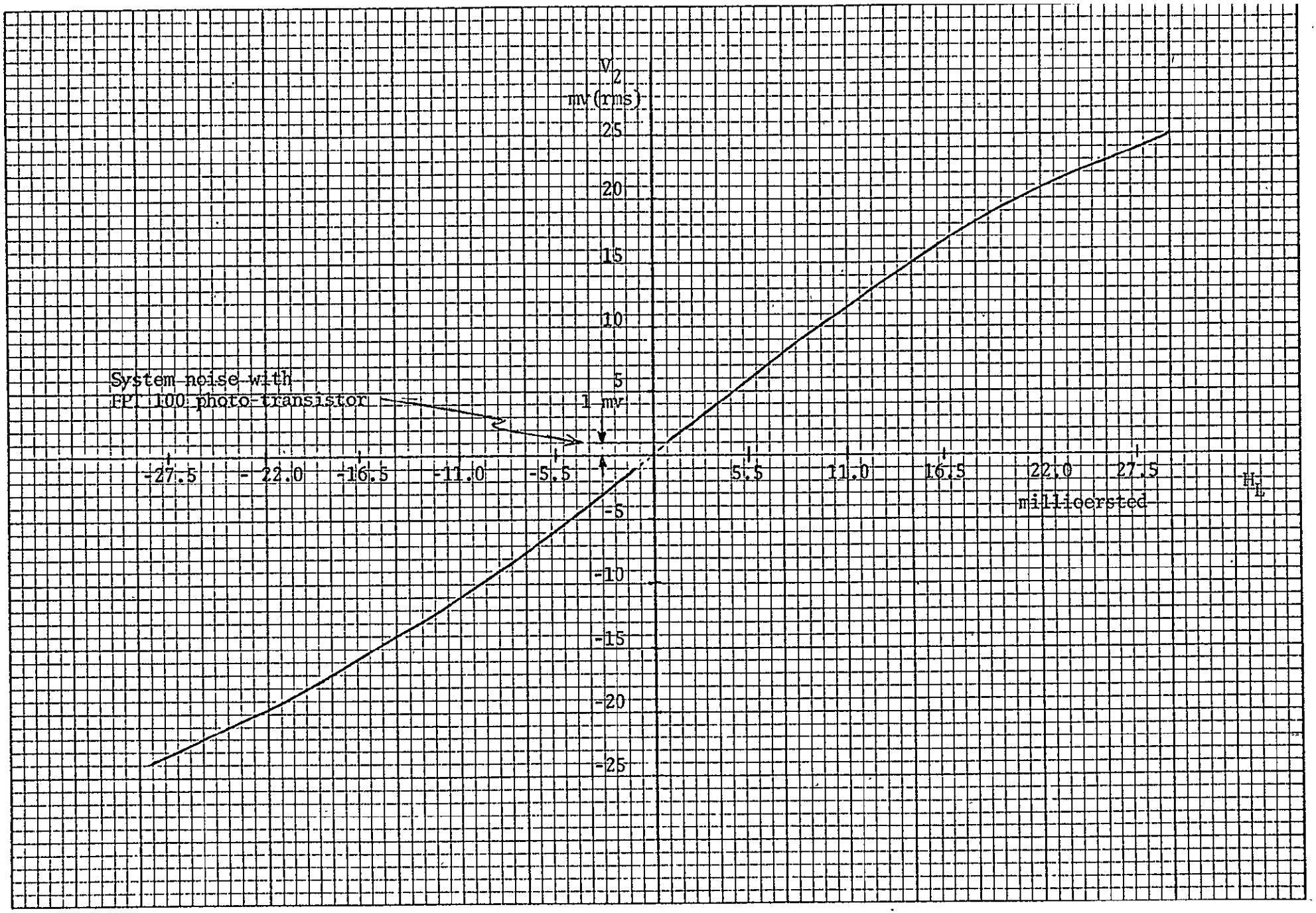

Fig. 4.1 Second Harmonic Voltage vs. Longitudinal Field

at the photo detector that is twice the frequency of the hard direction field drive frequency. The photo amplifier drives a narrow band ($\pm$ 30 hz) wave analyzer tuned at 1000 hz. The peak value of the 1000 hz photo amplifier signal is directly proportional to the applied longitudinal field. The photo amplifier voltage vs the applied field is given in Fig. 4.1.

APPENDIX

Kerr Null Position Calculation

The relations between the amplitudes of the electric field vectors, E_{pi}, E_{si}, in the incident wave and the amplitude of the electric field vectors, E_{pr}, E_{sr} in the reflected wave from a magnetized surface are

$$\begin{bmatrix} E_{sr} \\ E_{pr} \end{bmatrix} = \begin{bmatrix} r_{ss} & r_{sp} \\ r_{ps} & r_{pp} \end{bmatrix} \cdot \begin{bmatrix} E_{si} \\ E_{pi} \end{bmatrix} \qquad \text{(A1.1)}$$

where r_{ss} and r_{pp} are the ordinary Fresnel metallic reflection coefficients and r_{sp} and r_{ps} are the Kerr reflection coefficients.[11] In general, all of the reflection coefficients are complex. This relation can be considered a generalization of the well known Fresnel formula for metallic reflection from nonmagnetic surfaces, since for zero magnetization r_{sp} and r_{ps} vanish. For a magnetized surface the reflected beam contains a component that is, in general, both perpendicular and out of phase with the incident beam so that the reflected beam is elliptically polarized with the major axis of the ellipse rotated away from the incident polarization orientation.

The absolute values $|r_{sp}|$ and $|r_{ps}|$ are a measure of the ratio of the amplitudes of the Kerr components to that of the incident wave. Similarly, $|\frac{r_{sp}}{r_{ss}}|$ and $|\frac{r_{ps}}{r_{pp}}|$ are measures of their ratio to the corresponding amplitude reflected in the ordinary way. The tangents of the phase shift of the longitudinal K on components relative to the phase of the incident beam are given by

$$\tan \delta_k = - \mathrm{Im}(r_{sp})/\mathrm{Re}(r_{sp}) = \mathrm{Im}(r_{ps})/\mathrm{Re}(r_{ps}) \qquad \text{(A1.2)}$$

where Im and Re are the imaginary and real parts of the reflection coefficients respectively. The tangents of the phase shift of the Kerr components relative to

the components reflected in the ordinary way are given by

$$\tan \delta_{sk} = - \frac{\mathrm{Im}(\frac{r_{sp}}{r_{ss}})}{\mathrm{Re}(\frac{r_{sp}}{r_{ss}})} , \quad \tan \delta_{pk} = - \frac{\mathrm{Im}(\frac{r_{ps}}{r_{pp}})}{\mathrm{Re}(\frac{r_{ps}}{r_{pp}})} \tag{A1.3}$$

To avoid the ellipticity of the reflected beam due to non-p or non-s incident light, the Kerr instrument is set with approximately S incident light. However, the incident beam orientation is set experimentally by finding the smallest minimum transmission point for the polarizer and analyzer crossed. It will now be shown that this smallest minimum does not occur for pure S incident light.

To calculate the minimum transmission point or null position, assume the polarizer is oriented for approximately S light so that $(\frac{E_{pr}}{E_{sr}})$ and $(\frac{E_{pi}}{E_{si}})$ are small numbers. For this case, Eq. (A1.1) can be written as:

$$E_{sr} = r_{ss} E_{si} \tag{A1.4}$$

$$E_{pr} = r_{ps} E_{si} + r_{pp} E_{pi} \tag{A1.5}$$

or

$$r_{ss} \frac{E_{pr}}{E_{sr}} = r_{ps} + r_{pp} \frac{E_{pi}}{E_{si}} \tag{A1.6}$$

Since the incident light is plane polarized at a small angle ψ_o from the s axis, the ratio of the incident beam amplitudes is $\frac{E_{pi}}{E_{si}} = \psi_o$. For the null position the reflected beam must also be plane polarized for complete extinction by the analyzer. Therefore, set $\frac{E_{pr}}{E_{sr}} = \psi_r$, where ψ_r is the angle between the plane of polarization of the reflected beam and the s axis. Thus, Eq. (A1.6) becomes

$$r_{ss} \psi_r = r_{ps} + \psi_o r_{pp} \tag{A1.7}$$

Since $r_{ps} = -r_{sp}$ for the longitudinal Kerr effect, Eq. (A1.7) leads to the law of the reversibility between p light and s light for null rotation. The complex conjugate equation of Eq. (A1.7) can be written as

$$r_{ss}^* \psi_r = r_{ps}^* + \psi_o r_{pp}^* \tag{A1.8}$$

Solving Eqs. (A1.7) and (A1.8) simultaneously gives

$$\psi_o = \frac{r_{ss}^* r_{ps} - r_{ss} r_{ps}^*}{r_{ss} r_{pp}^* - r_{pp} r_{ss}^*} = - \frac{\mathrm{Im}\left(\frac{r_{ps}}{r_{ss}}\right)}{\mathrm{Im}\left(\frac{r_{pp}}{r_{ss}}\right)} = \frac{-|r_{ps}| \sin(\delta_k - \delta_s)}{|r_{pp}| \sin(\delta_p - \delta_s)}$$

$$\psi_r = \frac{r_{ps} r_{pp}^* - r_{pp} r_{ps}^*}{r_{ss} r_{pp}^* - r_{pp} r_{ss}^*} = \frac{\mathrm{Im}\left(\frac{r_{ps}}{r_{pp}}\right)}{\mathrm{Im}\left(\frac{r_{ss}}{r_{pp}}\right)} = \frac{|r_{ps}| \sin(\delta_k - \delta_p)}{|r_{ss}| \sin(\delta_s - \delta_p)}$$

Since ψ_o is not zero for magnetized materials the incident light is not pure s light. A similar calculation gives the same kind of result for approximately pp incident light due to the law of reversibility.

For the permalloy films used here the reflection coefficients have the following values,*

$|r_{ss}| = .80$ $\qquad$ $\delta_k - \delta_p = 105$ degrees

$|r_{pp}| = .6$ $\qquad$ $\delta_p - \delta_s = -229$ degrees

$|r_{ps}| = .71 \times 10^{-3}$ $\qquad$ $\delta_k - \delta_s = -124$ degrees

---

* See Ref. 5, p. 6.

which gives for a null

$\psi_o = 1.3 \times 10^{-3}$ radium polarizer setting

$\psi_r = 1.14 \times 10^{3}$ radium analyzer setting.

APPENDIX II

Photo Detector Magneto-optic Signal Calculation

A2.1 Domain States

There are two permutations of the basic domain states of the magnetized media that will be described here. These are

- Single domain
  - Magnetized parallel to plane of incidence
  - Magnetized at some angle out of the plane of incidence.
- Multidomain
  - Domains magnetized parallel to plane of incidence.
  - Domains magnetized at some angle out of the plane of incidence.

The magneto-optic signal derivations are based on Eqs. (3.2) and (3.3) of Sect. 3.2. In all cases, it is assumed the signal and not the contrast is important so θ is set such that $\theta >> \phi$ where θ is the angle of rotation of the analyzer from minimum transmission and ϕ is the Kerr effect angle. Therefore, the average light power is given by Eq. (3.4) for all of the different domain states. Also, only s polarized light is used to avoid the transverse Kerr effect.

A2.2 Single Domain State

Although the magneto-optic signal for the magnetic media switched from one single domain state to the opposite state has been derived elsewhere, it is rederived here to compare with the multidomain state switching signal.[6] From Eqs. (3.2) and (3.3) the magneto-optic signal for single domain switching

can be written as

$$\Delta W = I_o \, t \, A_T \, [\sin^2(\theta + \phi) - \sin^2\theta] \qquad \text{(A2.1)}$$

where all of the symbols are defined in Sect. 3.2. From a trigonometry identity

$$\sin^2(\theta+\phi) = \sin^2\theta \cos^2\phi + 2 \sin\theta \cos\theta \sin\phi \cos\phi + \sin^2\phi \cos^2\theta \qquad \text{(A2.2)}$$

and since for the magnetic media to be considered $\phi \sim 10^{-3}$ to 10^{-2} radians

$$\cos\phi \simeq 1 \quad \text{and} \quad \sin\phi \simeq \phi$$

so

$$\sin^2(\theta+\phi) = \sin^2\theta + \phi \sin 2\theta \qquad \text{(A2.3)}$$

This gives

$$\Delta W = I_o \, t \, A_T \, \phi \sin 2\theta \qquad \text{(A2.4)}$$

In the case of the domain magnetized parallel to the plane of incidence, the Kerr effect angle, ϕ , is equal to the maximum for that particular magnetic material plus entrancement coatings. Let this Kerr effect angle be called ϕ_m . Since $\phi = \phi_m$ which is constant, the magneto-optic signal varies only with light intensity for a particular analyzer setting.

In the case where the domain is not saturated at an angle out of the plane of incidence by some angle α as shown in Fig. A2.1, then the magnetization component parallel to the plane of incidence (p of i)

$$M_p = M_s \cos\alpha \qquad \text{(A2.5)}$$

where M_s is the saturation magnetization. Since the Kerr effect angle is proportional to M_p the following equation can be written

$$\frac{\phi}{\phi_m} = \frac{M_p}{M_s} = \cos \alpha \tag{A2.6}$$

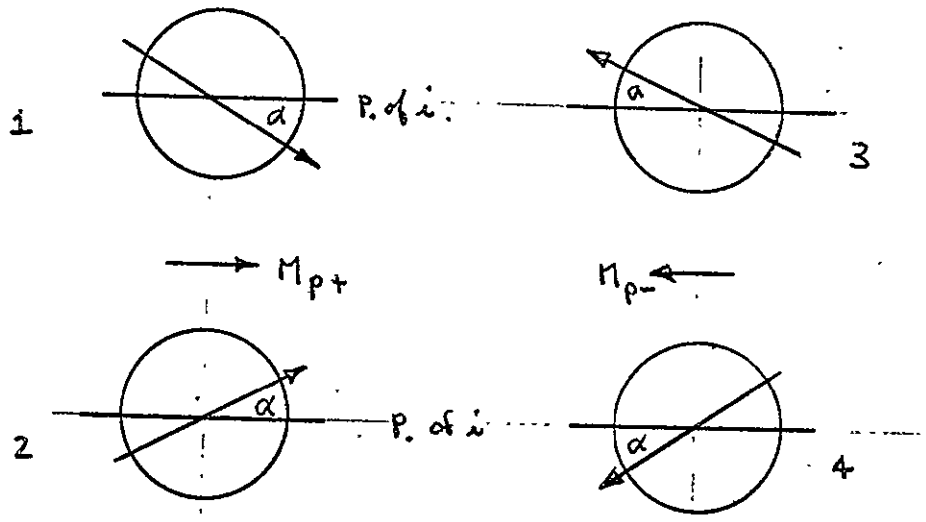

Fig A2.1 Single Domain States

Thus, the magneto-optic signal becomes

$$\Delta W = I_o \, t \, A_T \, (\phi_m \cos \alpha) \sin 2\theta \tag{A2.7}$$

where the switching occurs from states 1 or 2 to states 3 or 4 shown in Fig. A2.1. Since Eq. (A2.7) equals Eq. (A2.4) when $\alpha = 0$, then Eq. (A2.7) can be considered as a generalized magneto-optic signal equation for single domain switching. Note as indicated by Fig. A2.1 for $\alpha > 0$, the initial and final domain states cannot be determined from the magneto-optic signal alone since all the following state transistions give the same magneto-optic signal.

state 1 ⟶ state 3

state 1 ⟶ state 4

state 2 ⟶ state 3

state 2 ⟶ state 4

A2.3 Multidomain State

The multidomain case for domains saturated parallel to the plane of incidence is derived in Sect. 3.2, Eq. (3.7). The effect of domains saturated at an angle α to the p , of i can be handled the same way as the single domain case where

$$\phi = \phi_m \cos \alpha \tag{A2.8}$$

This gives

$$\Delta W = \frac{I_o t}{2} \Delta A(\phi_m \cos \alpha) \sin 2\theta \tag{A2.9}$$

as the generalized magneto-optic signal equation where the effects of both the differential domain area, ΔA , and the orientation of the domains relative to the p of i , α , are included. Eq. (A2.9) can also be used to describe single domain switching if ΔA is set equal to $2A_T$, which is the total range of ΔA .

There are other multidomain switching configurations, e.g. ripple within a domain, that could be analyzed but it was felt they are not of as much general interest as the domain configurations considered. The magneto-optic signal equations for other domain configurations can be developed using this same general approach.

APPENDIX III

Light Radiant Power Calculation

A3.1 Arc Radiant Power

The light source for the Kerr instrument is a 75 watt xenon short arc lamp. A complete set of lamp specifications is given in Appendix 4. The luminance distribution between the anode and cathode is assumed to be the same as that given by Hewitt and Vause[12], as shown in Fig. A3.1. The average luminance over the electrodes is calculated to be approximately 96×10^3 candela/cm^2 which compares with the data given on the 75 watt xenon used here. Assuming a spectral luminous efficiency of 680 lumen/watt,[13] the radiant power for an arc area of $.935\ 10^{-3}$ cm^2 is

$$I = 10^5 \frac{\text{lumen}}{\text{steradian - cm}^2} \times \frac{\text{watt}}{680 \text{ lumen}} \times .935\ 10^{-3}\ \text{cm}^2$$

$$I = 138 \text{ milli watts/steradian}$$

A3.2 Condenser

A double lens condensing system, as shown in Fig. A3.2, was used to produce a parallel beam. For the cone angle shown the solid angle subtended by the first condenser is $.2\pi$ steradian. Assuming a lens transmission coefficient of .5 gives a transmitted light power through the first condenser of 43 milliwatts. Since the cone angle of the first condenser is less than the cone angle of the arc lamp, the average luminance over the lens area is assumed to be uniform at 138 mw/steradian.

The arc image is formed at 6.6 inches from the first condenser with a cone angle of 15 degrees. Since the collection angle of the second condenser is 18.3 degrees all of the transmitted light is collected at the second condenser. The second condenser is positioned so that its' focal point is slightly to the left

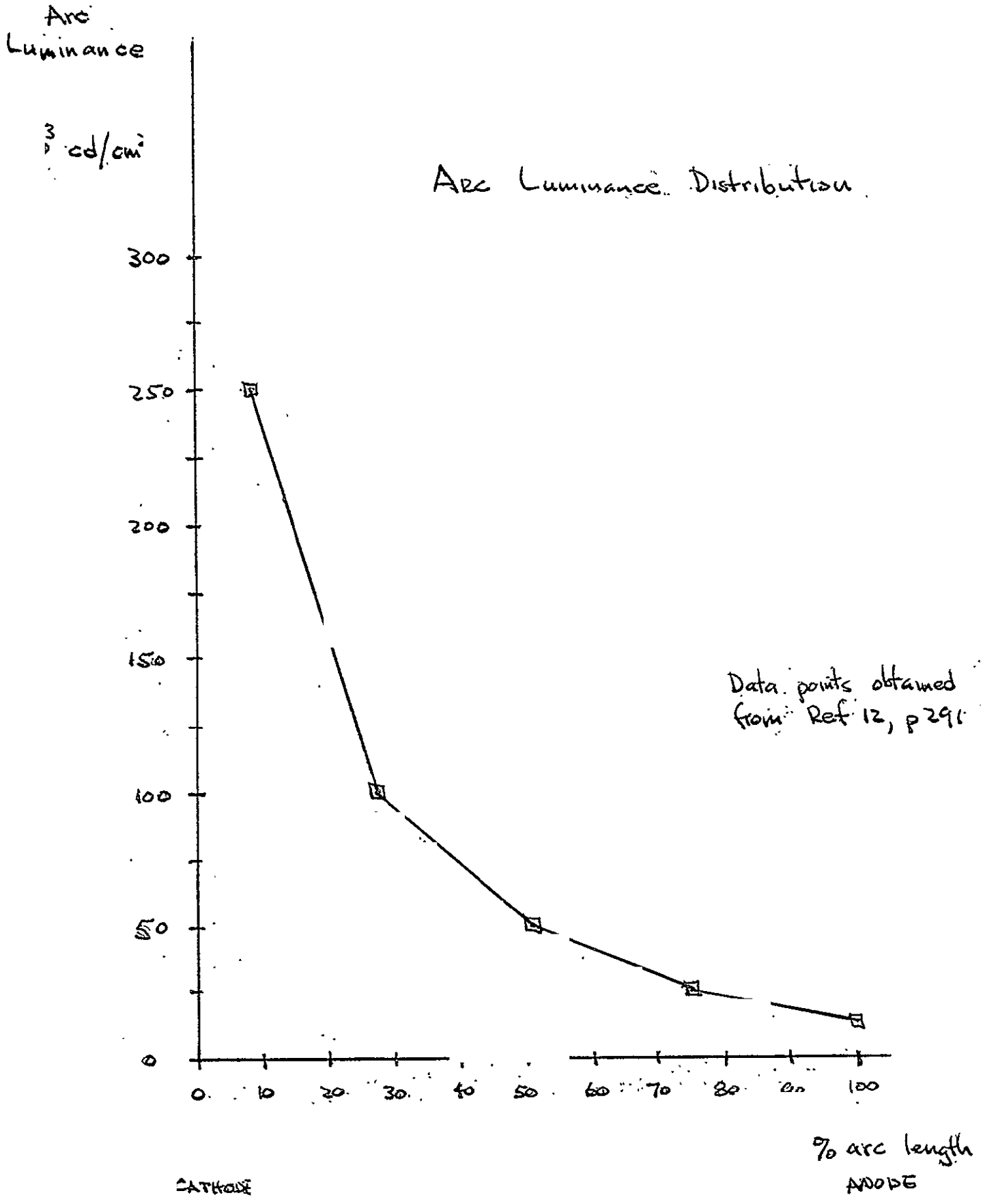

Fig. A3.1 Xenon Arc Luminance

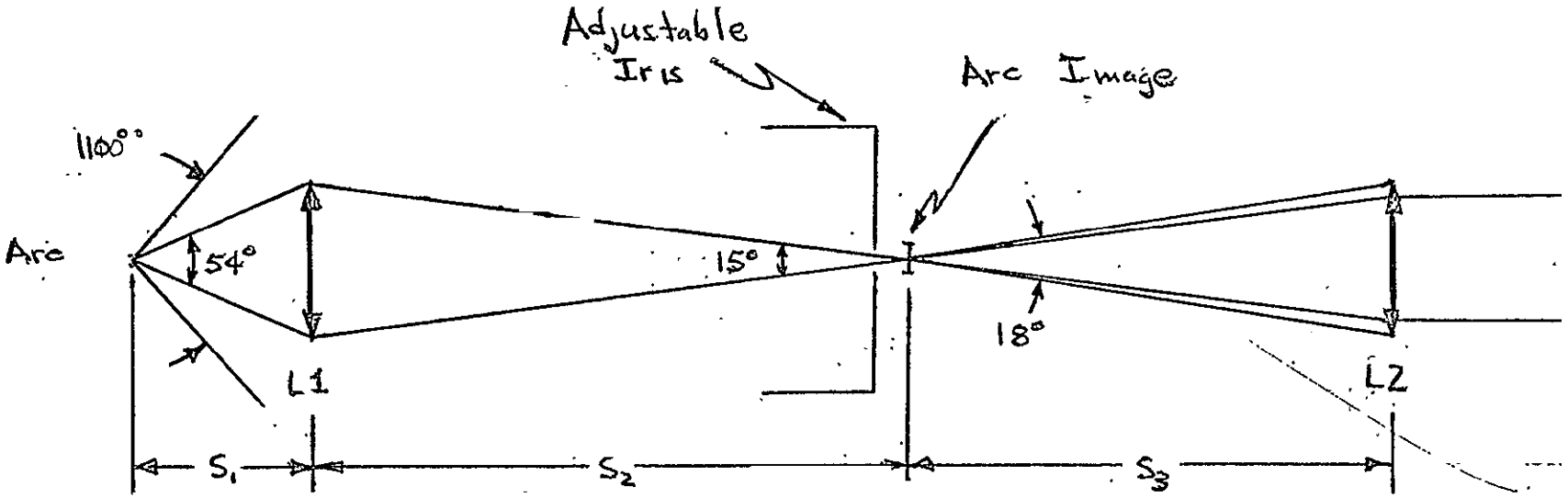

$S_1 = 1.94''$
$S_2 = 6.6''$
$S_3 = 4.9''$

L1 - F 1.5", a 1.75"

L2 - F 4.95", a 1.58"

Fig. A3.2 Condenser

of the arc image at about the point of maximum brightness.[14]

Since the arc image is effectively the light source for the second condenser the divergence of the parallel beam is determined by the arc image size. The beam divergence, γ , for an arc image of .0408 inches is

$$\gamma = \tan^{-1} \frac{.0408}{4.95} = .46 \text{ degrees.}$$

Since γ is so small the beam will be assumed to be ideally parallel. The maximum diameter of the beam transmitted through the second condenser is given by

$$2(4.95) \cos 7.55^{o} = 1.3 \text{ inch} = 3.32 \text{ cm}$$

The maximum radiant transmitted power in the beam is $2.1\ 10^{-3}$w after the .5 lens transmission coefficient is included. The radiant power in a 1.0 cm diameter beam is given by

$$W_1 = \left(\frac{1 \text{ cm}}{3.32 \text{ cm}}\right)^2 21 \text{ mw} = 1.9 \text{ mw}$$

This beam is transmitted to the polarizer.

A3.3 Polarizer - Analyzer

Since the 1 cm diameter beam incident on the Glan Thompson prism polarizer is unpolarized, the transmission coefficient is .45 . Therefore, the radiant power incident on the magnetic media surface from the polarizer is .75 mw. Because the light beam is polarized perpendicular to the plane of incidence (s light) and the Fresnel metallic reflection coefficient of Ni-Fe for s light in the visible region is about..80, the radiant power, W_a, reflected to the analyzer is about .48 milliwatts.

A3.4 Magneto-optic signal radiant power

As shown by Eq. (3.4) the average radiant power transmitted by the analyzer set at $\theta = 10^{o}$ and incident on the photo-detector is given by

$$W_r = W_a \, t \sin^2\theta = 7.5 \times 10^{-6} \text{ watts}$$

where t is the focusing lens transmission coefficient.

The magneto-optic signal radiant power for the film completely magnetized in one direction is given by Eq. (3.7) to be

$$\Delta W = W_a \, t \, \phi \sin 2\theta = 42 \times 10^{-9} \text{ watts}$$

for a Kerr angle, $\phi = 10^{-3}$ radian.

This calculation only gives the order of magnitude of the radiant power since the detailed spectral response of the optical components and the Kerr effect over total frequency range of the xenon arc lamp not included. To be conservative, all of the transmission coefficients and reflection coefficients were taken to the pessimistic side.

REFERENCES

1. M. Prutton, Thin Ferromagnetic Films, Butterworths, London, (1964).

2. C. A. Fowler and E. M. Fryer, Magnetic Domains by the Longitudinal Kerr Effect, Phys. Rev., 94, 52 (1954).

3. C. A. Fowler, E. M. Fryer, D. Treves, Observations of Domains in Iron Whiskers under High Fields, Jour. Appl. Phys., 31, 2267 (1960).

4. D. Treves, Limitations of the Magneto-optic Kerr Technique in the Study of Microscopic Magnetic Domain Structures, Jour. Appl. Phys., 32, 358 (1961)

5. G. Fan, E. Donath, E. S. Banakette, A. Wirgin, Analysis of a Magneto-optic Readout System, I.E.E.E., EC 12, 3 (1963).

6. D. Treves, Magneto-optic Detection of High Density Recordings, Jour. Appl. Phys., 38, 1192 (1967).

7. P. H. Lissberger, Kerr Magneto-optic Effect in Ni-Fe Films, I. Experimental, Jour. Opt. Soc. Amer., 51, 957 (1961).

8. C. C. Robinson, Longitudinal Kerr Magneto-optic Effect in Thin Films of Fe, Ni, and Permalloy, Jour. Opt. Soc. Amer., 53, 681 (1963).

9. T. Yoshino, S. Tanaka, Longitudinal Magneto-optic Effect in Ferrimagnetic Thin Films, I, Jour. Appl. Phys. (Japan), 5, 994 (1966).

10. F. A. Jenkins and H. E. White, Fundamentals of Optics, McGraw-Hill, 3rd Ed. 1957.

11. A. V. Sokolov, Optical Properties of Metals, Amer. Elsevier Publ., New York, p. 268 (1967).

12. H. Hewitt and A. S. Vause, Lamps and Lighting, American Elsevier Publishing Company, New York, 1966, p. 291.

13. G. A. Condas, Maximum Spectral Luminous Efficiency, Journal Opt. Soc. Amer., 54, 1168, 1964.

14. H. A. Keitz, Light Calculations and Measurements, Philips Technical Library, 1955, p. 192.